SNO-STR-99-007

High Intensity Laser Timing and Air Fill Muons at SNO

Rob Hanson

Supervisor: *Dr. J. Law*

Prepared for Dr. C. Fischer
76-451 Advanced Physics Project
Department of Physics
University of Guelph
Guelph, Ontario

5 April, 1999

I. Introduction

The Sudbury Neutrino Observatory (SNO) is a heavy water Cherenkov detector located 2070m below ground in Inco's Creighton Mine, where 10 000 photomultiplier tubes (PMTs) sensitive to Cherenkov photons view 1000 tonnes of heavy water (D_2O) as a target for solar neutrinos. The D_2O is contained in a 12 m diameter acrylic vessel surrounded by a 17 m diameter geodesic sphere on which the 10 000 20 cm PMTs are mounted.[1] The remainder of the 22 m diameter barrel-shaped detector cavity is filled with ultra-pure light water to shield background radiation and to provide mechanical support for the acrylic vessel. Although primarily designed to study solar neutrinos, the SNO detector will also be sensitive to supernova generated and atmospheric neutrinos, as well as cosmic ray muons.

A. The Solar Neutrino Problem

There has always been a large deficit in the number of solar electron neutrinos measured by previous neutrino detectors compared to the number that the Standard Solar Model predicts. There is abundant evidence that the Standard Solar Model is otherwise correct, so the currently accepted hypothesis is that the electron neutrinos produced by fusion reactions in the sun are oscillating into one of the other two types (or 'flavours') of neutrino en route to the earth.[2] If this is true, it would require that neutrinos have mass. SNO is unique in that it will be the only detector capable of detecting all three flavours of neutrino, and by measuring the ratio of electron neutrinos to the total number of neutrinos should provide an answer to what is known as "The Solar Neutrino Problem". A non-zero neutrino mass would not only impact our theories of fundamental particle interactions, but would also have profound cosmological consequences.

B. Neutrino Detection

SNO will detect neutrinos by three main reactions.[3] The first reaction is the type employed by other light water neutrino detectors, elastic electron-neutrino scattering:

$$\nu_x + e^- \rightarrow \nu_x + e^- \qquad (1)$$

Although sensitive to all flavours of neutrino (denoted by ν_x), the electron neutrino is largely dominant in this type of reaction. The second reaction, sensitive to electron neutrinos only, is known as the 'charged current reaction':

$$\nu_e + d \rightarrow p + p + e^- \qquad (2)$$

When the deuterium nucleus absorbs a neutrino, a high energy electron is produced. In both (1) and (2), the electron on the right hand side of the equation is moving fast enough that it produces detectable Cherenkov radiation in the detector. The last type of reaction is sensitive to all flavours of neutrino. The neutral current reaction involves deuteron disintegration as follows

$$\nu_x + d \rightarrow \nu_x + p + n \qquad (3)$$

When the neutron that is produced is absorbed by another nucleus, an energetic gamma ray is emitted, which produces detectable Cherenkov radiation.

The number of photons reaching the PMTs and the time at which they reach them are used to determine the energy and position of neutrino interactions, so accurate time and charge measurement calibrations are of crucial importance. In the first part of this research, optical calibration data from a laser source is examined.

II. Optical Calibration

To check the gain and efficiency of the individual PMTs, as well as other optical effects within the detector (for example the effect of the acrylic vessel), a nitrogen dye laser is used as a source of optical photons. The laser is located externally to the detector, and linked to an isotropic scattering ball within the detector via fibre optic cables. In the first part of this analysis, time and charge spectra for high intensity air-fill laser runs are examined in detail, and compared to Monte-Carlo simulations. Although well out of the range of typical solar neutrinos, high charge PMT response is of some interest as cosmic ray muons and nearby supernovae would produce light in the detector of similar intensity.

Figure 1 shows the timing spectrum for all channels for a typical high intensity laser run; the y-axis is the number of PMTs that fired for a given time. The most dominant peak, labelled 1, corresponds to light travelling directly from the laser source in the centre of the detector to the PMT support structure. The time of ~130 ns for this peak is dominated by laser-PMT photon transit time, electron transit time in the PMT, and delay due to cable length. Peak two occurs as a result of light reflecting off of the inside of the empty acrylic vessel and hitting the opposite side of the PMT support structure, while peak three corresponds to light reflected off of the PMT support structure itself, causing PMTs to fire

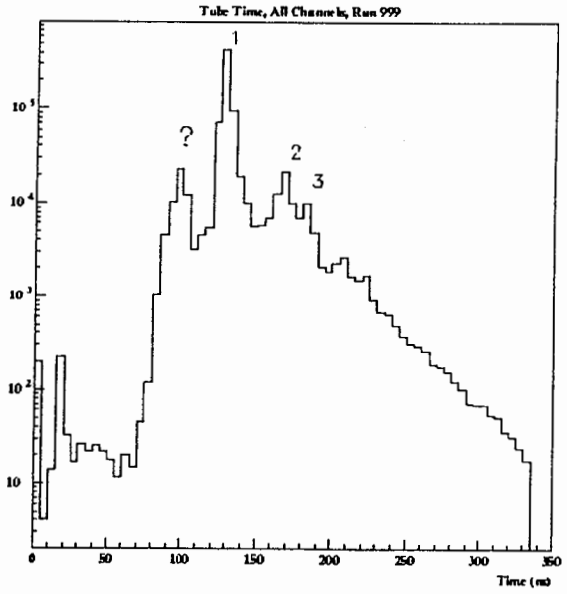

Figure 1: High Intensity Laser Timing Spectrum.

on the opposite side. Second order reflection peaks are also visible at roughly 200 - 220 ns. The peak labelled with the question mark has been seen before, and is not unique to this particular run. One hypothesis is that it is a result of PMT prepulsing, an effect whereby a photon passes directly through the photocathode of the PMT and strikes the dynode chain directly. The difference in transit times between the photocathode and the dynode chain between a photon and an electron is on the order of 20 - 30 ns, depending on where the photon strikes the dynode chain. This is a well documented property of the SNO PMTs, and is believed to occur to roughly 1% of the photons striking the PMTs. High intensity laser data is well suited to study this phenomenon because, due to the large number of photons involved, this 1% effect becomes more readily visible.

Figure 2 show a plot of the charge output of all of the PMTs as a function of time. Events with higher charge correspond to events with more light in the detector. If prepulsing occurs 1% of the time, then more photons should result in more early prepulsing events. Figure 2 however shows that the opposite is true.

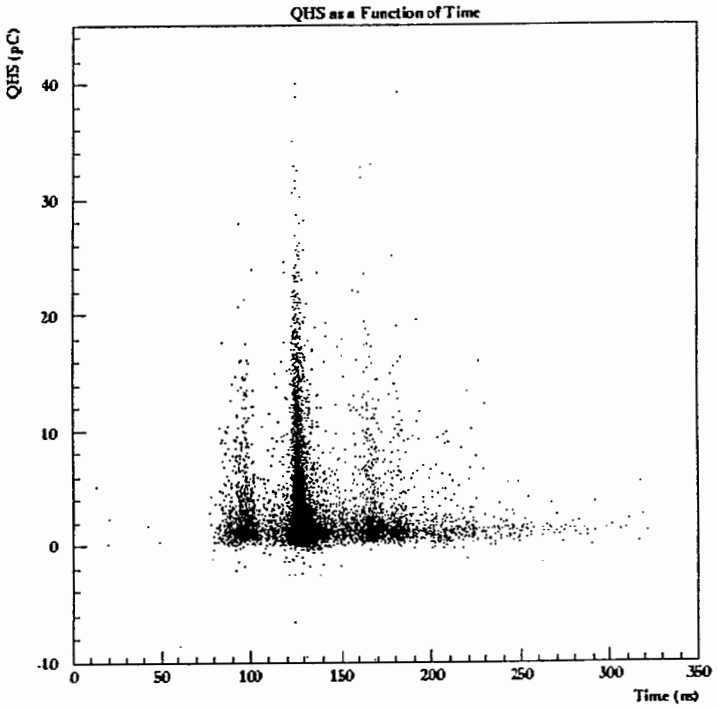

Figure 2: Charge as a Function of Time

The group of early events at roughly 100 ns is clearly visible, however the number of early events does not increase as the number of photons increases. The early peak disappears completely in figure 3, which shows the uncalibrated time spectrum for the same laser

run in raw ADC counts. Note that in this case the shape of the spectrum is reversed; higher ADC counts correspond to earlier time. This supports the conclusion that the early peak is a problem with timing calibration constants in the electronics rather than a physical problem with the PMTs themselves. Closer analysis of the calibrated timing spectra on a channel by channel basis further supported the conclusion that the early peak was not due to prepulsing; the early signal was found to be originating in only a few (roughly 500) of the electronics channels. These calibrations have since been corrected, and the timing spectra are back to normal.

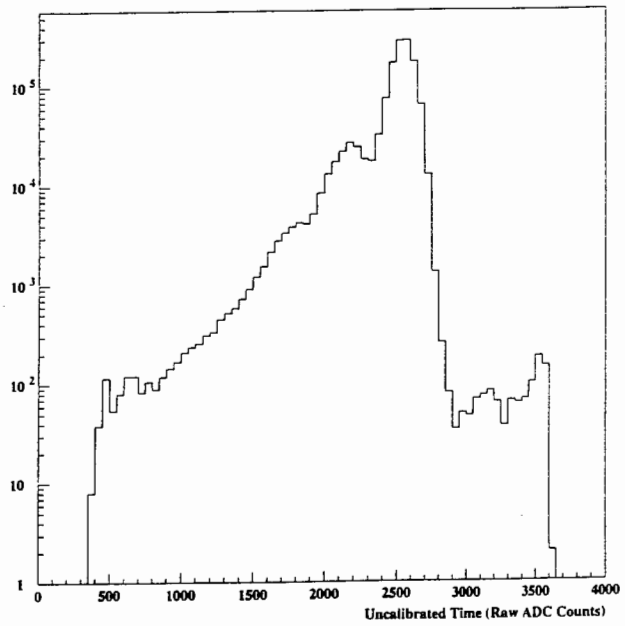

Figure 3: Uncalibrated Time Spectrum

III. Cosmic Ray Muons

Muons formed as a result of high energy cosmic rays interacting with atmospheric nuclei constitute a significant high energy background signal for SNO, and are one of the reasons that the detector is located beneath 2 km of solid rock. One of the consequences of being so far underground is that only very high energy cosmic ray muons actually reach the SNO detector, typically with energies on the order of 500 GeV.[4] At this energy, the muons are moving fast enough to produce detectable Cherenkov radiation as they pass through the acrylic of the empty heavy water vessel, thus

representing a unique chance to evaluate the detector's response to Cherenkov radiation before it is filled with water. In the second part of this analysis, the detector's sensitivity to muon-induced Cherenkov photons is evaluated and compared to simulations, and an attempt is made to measure the energy spectrum of the air fill muons seen.

A. Detector Efficiency

When a muon passes through the acrylic of the acrylic vessel, a cone of Cherenkov radiation is produced. However, only half of this cone escapes the acrylic; the other half is totally internally reflected (See Figure 4). When this half-cone reaches the PMT support structure, the PMTs that fire form a semicircle pattern. Hence, two semicircles are visible in the final PMT hit pattern; one from the muon entering the AV and one from the muon leaving the AV. Figure 5 shows the x-y projection of the hit pattern of a simulated 500 GeV muon travelling straight down through the detector, 2 m along the x-axis. This is essentially the bottom view of the PMT support structure, showing all of the tubes that fired. The larger ring is from the muon entering the AV, the smaller

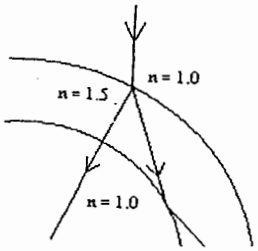

Figure 4: Total Internal Reflection in Acrylic

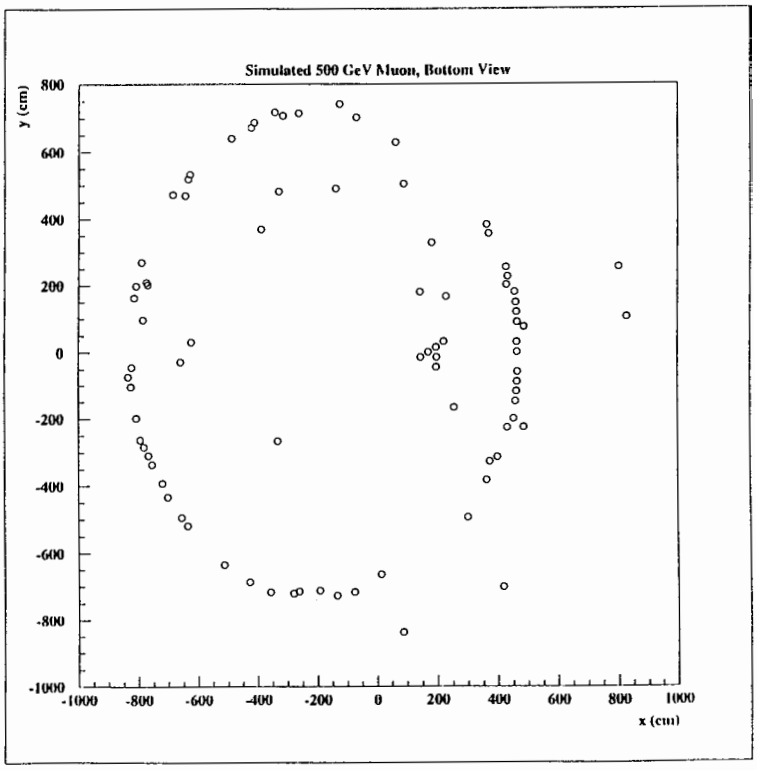

Figure 5: Simulated 500 Gev Muon

more well defined ring is the AV exit, and the small cluster of PMTs at x=200, y=0 is the point at which the muon exited the PMT support structure.

A first order estimate of the detector's efficiency with at detecting Cherenkov photons can be obtained by simple direct comparisons between the real muon data and Monte-Carlo simulated air-fill muons. Since the number of tubes hit in the AV entry and exit rings is proportional to the number of Cherenkov photons detected, if the number of tubes in the rings are the same in the real data as they are in the simulation, then the detector is indeed as sensitive to Cherenkov photons as was originally thought. Since the AV exit ring is in general more clearly defined, it was used as the comparison. Figure 6 (a) shows that the mean number of tubes in the AV exit ring for the

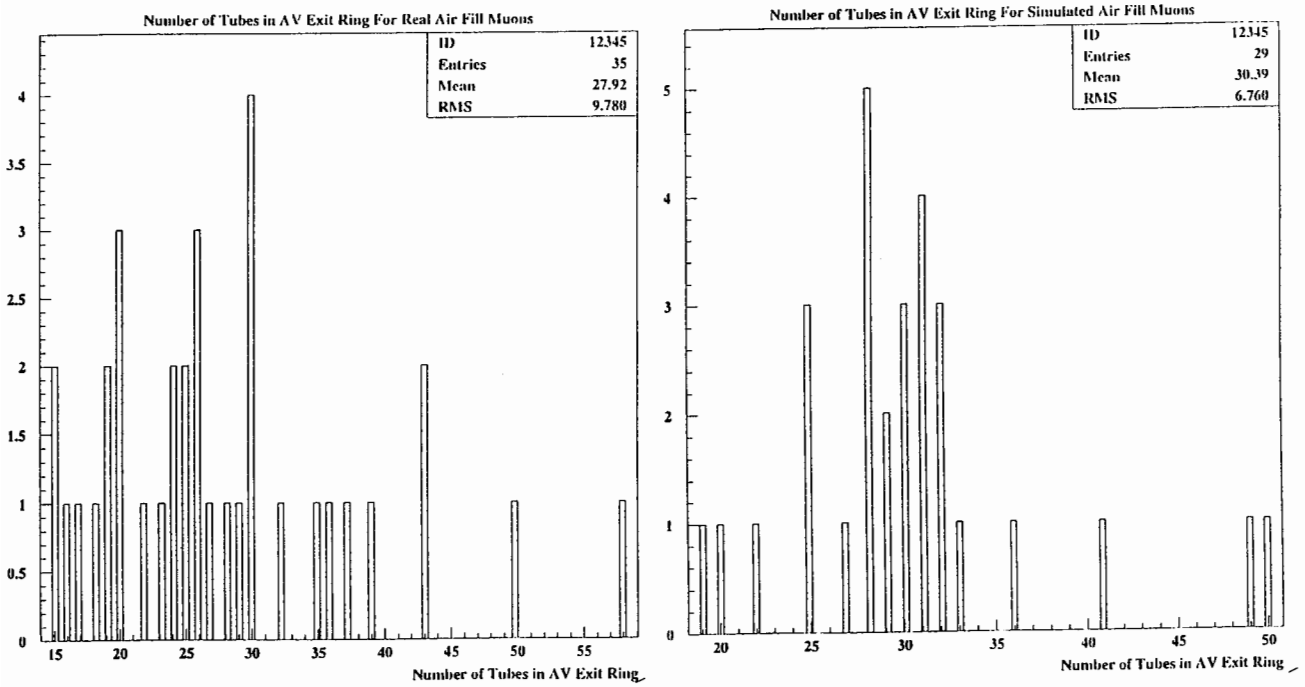

Figure 6: Number of PMTs in AV Exit Ring for (a) Real and (b) Simulated Muons

real air-fill muons was 27.92. In figure 6 (b), we see that the mean number of tubes in the AV exit ring for equivalent simulated muons is 30.39. These values are in reasonable agreement without even taking into account that 10-15 % of the PMTs were not operational when the real data was taken. If this had been reflected in the simulation, the agreement would be even better.

B: Measurement of Air-Fill Muon Energy Spectrum

There are two approaches used here to determine air-fill muon energy at SNO. Both attempt to measure the velocity of the incident muon, then use relation (4) to calculate the energy:

$$E^2 = p^2c^2 + m_o^2c^4 \qquad (4)$$

The first method involves measuring the speed of the muon through the acrylic vessel by using the timing of the PMTs that fire when the muon enters and exits the AV. By fitting a circle to the hit pattern of tubes corresponding to the muon's entry and exit, the trajectory of the muon can be obtained by connecting a line

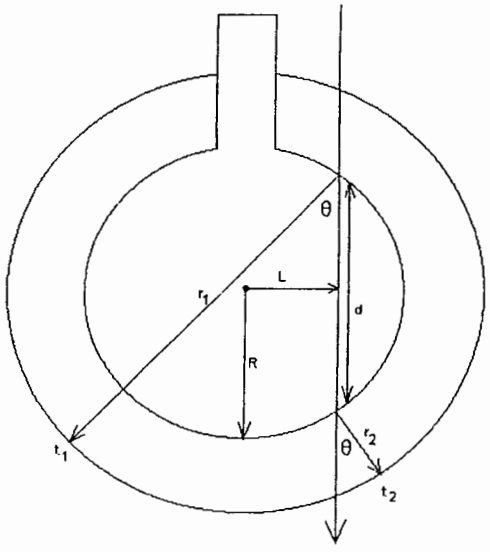

Figure 7: Geometry Overview

between the centres of the circles. Once the trajectory is known, the exact coordinates of the points where the iew muon interacted in the acrylic can be found, as can the distance travelled in the AV. The absolute AV entry and exit times can be determined from the PMT firing times by subtracting the average time it takes the light to travel from the interaction point in the acrylic to the corresponding PMTs. Knowing the entry and exit times and the distance travelled in the acrylic vessel allows calculation of the muon's velocity. From figure 7 we have that

$$v = 2\frac{\sqrt{R^2 - L^2}}{t_2 - t_1 + \frac{1}{c}(\vec{r}_1 - \vec{r}_2)}$$

This method is limited by the timing resolution of the PMTs, which is on the order of 1 ns. Unfortunately, this severely limits the usefulness of this method for muon energies higher than approximately 1 GeV. As figure 8 shows, the difference in AV transit times for muons with energy higher than a GeV becomes much less than one ns, which results in large errors in velocity measurements. Using simulated muons of 200 MeV, it is possible to measure the energy to within 6% accuracy using this method. The error becomes roughly 23% at 1 GeV, and increases extremely rapidly after that.

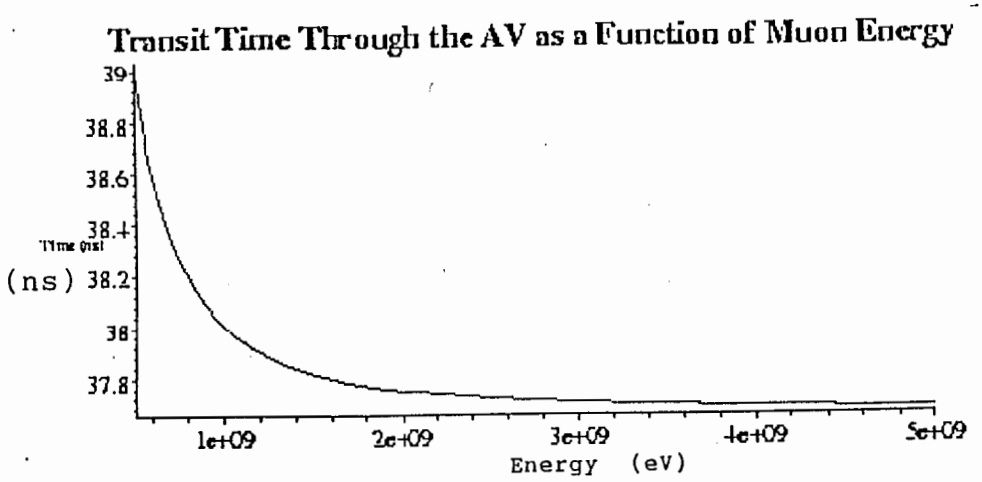

Figure 8: AV Transit Time as a Function of Muon Energy

The second method for measuring muon velocity involves measuring the angle of the Cherenkov cone, and thus is not limited by the timing resolution of the PMTs. The angle of the Cherenkov cone produced by a high energy particle depends on the index of refraction of the medium and the velocity of the particle in the following way:

$$\theta = \arccos\left(\frac{1}{n\beta}\right)$$

If the muon trajectory is fit in the same way as the previous method, then knowing the radius of curvature of the ring and the coordinates of the corresponding interaction point in the acrylic vessel allows the Cherenkov angle to be calculated. The velocity of the muon follows:

$$v = \frac{c}{n(\cos\theta)}$$

Unfortunately, this method falls also falls apart at high muon energies. In this case, the problem is one of geometry rather than timing.

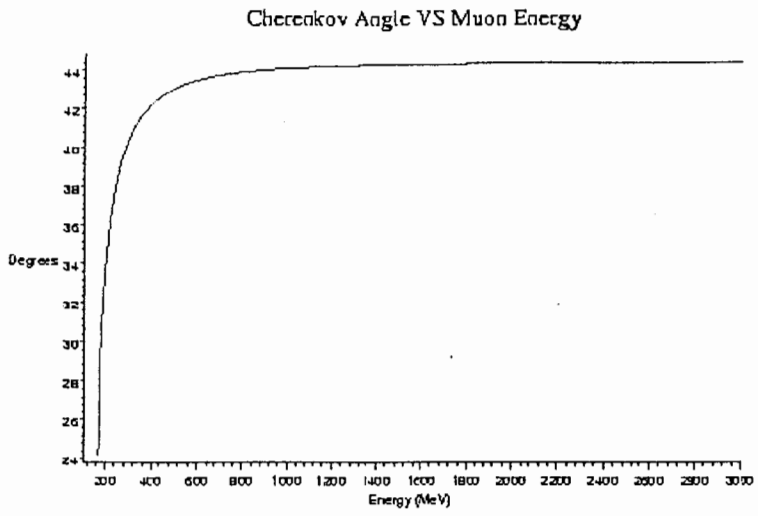

Figure 9: Cherenkov Angle as a Function of Muon Energy

Figure 9 shows Cherenkov angle as a function of muon energy. The angle becomes rapidly asymptotic at energies higher than 1 GeV, which is much less than the energy that most muons in the detector will have.

Although it would have been interesting to measure the energy spectrum of the air-fill muons, the detector was never really designed for air-fill operation, so it is not surprising that these methods had trouble. Once the detector is full of water, the signs of a muon in the detector become vastly different, so spending a large amount of time developing a more robust method of determining air - fill muon energies is of limited usefulness.

IV. Conclusions

Preliminary analysis of charge and time spectra from high intensity optical calibration runs with the nitrogen dye laser showed very good agreement between the real data and simulations. With the exception of a few anomalous channels that have since been corrected, the detector is for the most part responding exactly as expected to higher than average levels of light.

Analysis of air-fill cosmic-ray muons is interesting as it provides an early way to study detector response to real physics. A direct comparison between simulated muons and real data yields very good agreement; the detector's sensitivity to Cherenkov photons is, at least initially, exactly as expected. Attempts at measuring the energy of air-fill muons met with limited success in all but the very lowest energy cases. This does not present a problem though; it is not critical that the detector be very sensitive to air-fill physics, and the properties of muons in the detector change dramatically when it is full of water.

V. References

[1.] Cowen, D. F. *et al.* **The Sudbury Neutrino Observatory Electronics Chain**, *IEEE Transactions on Nuclear Science*, 1995, **42**, No. 4, 925.

[2.] Chon, M. C. **Muon Physics and Neural Network Event Classifier for the Sudbury Neutrino Observatory**, Ph. D. Thesis, University of Guelph, 1997.

[3.] Ewan, G. T. *et al.*, **Sudbury Neutrino Observatory Proposal**, SNO-87-12, October 1987.

[4.] Taylor, J. R. and C. Zafiratos, **Modern Physics for Scientists and Engineers.** Prentice Hall, New Jersey, 1991.